

OFDM Achieves the Lowest Ranging Sidelobe Under Random ISAC Signaling

Fan Liu, *Senior Member, IEEE*, Ying Zhang, *Student Member, IEEE*,
Yifeng Xiong, *Member, IEEE*, Shuangyang Li, *Member, IEEE*, Weijie Yuan, *Senior Member, IEEE*,
Feifei Gao, *Fellow, IEEE*, Shi Jin, *Fellow, IEEE*, and Giuseppe Caire, *Fellow, IEEE*

Abstract—This paper aims to answer a fundamental question in the area of Integrated Sensing and Communications (ISAC): *What is the optimal communication-centric ISAC waveform for ranging?* Towards that end, we first established a generic framework to analyze the sensing performance of communication-centric ISAC waveforms built upon orthonormal signaling bases and random data symbols. Then, we evaluated their ranging performance by adopting both the periodic and aperiodic auto-correlation functions (P-ACF and A-ACF), and defined the expectation of the integrated sidelobe level (EISL) as a sensing performance metric. On top of that, we proved that among all communication waveforms with cyclic prefix (CP), the orthogonal frequency division multiplexing (OFDM) modulation is the only globally optimal waveform that achieves the lowest ranging sidelobe for quadrature amplitude modulation (QAM) and phase shift keying (PSK) constellations, in terms of both the EISL and the sidelobe level at each individual lag of the P-ACF. As a step forward, we proved that among all communication waveforms without CP, OFDM is a locally optimal waveform for QAM/PSK in the sense that it achieves a local minimum of the EISL of the A-ACF. Finally, we demonstrated by numerical results that under QAM/PSK constellations, there is no other orthogonal communication-centric waveform that achieves a lower ranging sidelobe level than that of the OFDM, in terms of both P-ACF and A-ACF cases.

Index Terms—Integrated Sensing and Communications, OFDM, auto-correlation function, ranging sidelobe.

I. INTRODUCTION

ENVISIONED as a transformative paradigm, the sixth generation (6G) of wireless networks is set to drive forward emerging applications such as autonomous vehicles, smart factories, digital twins, and low-altitude economy [1], [2]. This new era of connectivity will extend beyond traditional communication roles, ushering in the ISAC technology [3]. Notably, the International Telecommunication Union (ITU) has recently endorsed the global 6G vision, highlighting ISAC as one of its six primary usage scenarios [4].

F. Liu, Y. Zhang, and W. Yuan are with the School of System Design and Intelligent Manufacturing, Southern University of Science and Technology, Shenzhen 518055, China. (e-mail: liuf6@sustech.edu.cn, yuanwj@sustech.edu.cn, yingzhang98@ieee.org).

Y. Xiong is with the School of Information and Electronic Engineering, Beijing University of Posts and Telecommunications, Beijing 100876, China. (e-mail: yifengxiong@bupt.edu.cn)

S. Li and G. Caire are with the Chair of Communications and Information Theory, Technical University of Berlin, 10623 Berlin, Germany (e-mail: shuangyang.li@tu-berlin.de, caire@tu-berlin.de).

F. Gao is with the Department of Automation, Tsinghua University, Beijing 100084, China (e-mail: feifeigao@ieee.org).

S. Jin is with the National Mobile Communications Research Laboratory, Southeast University, Nanjing 210096, China (e-mail: jinshi@seu.edu.cn).

The core concept of ISAC in 6G networks is to leverage wireless resources such as time, frequency, beam, and power across both sensing and communication functionalities using a unified hardware platform [5]. The main challenge in ISAC lies in developing a dual-functional waveform that can effectively handle both target information acquisition and communication information delivery over the ISAC channel [6], [7], which generally follows three design philosophies: sensing-centric, communication-centric, and joint designs [3]. While the sensing-centric methodology aims at embedding communication information into existing radar sensing waveforms, e.g., chirp signals, its communication-centric counterpart seeks to implement sensing over standardized communication signaling schemes. In contrast to those, the joint design approach creates novel ISAC waveforms from scratch, aiming to balance and optimize the tradeoff between sensing and communication [8].

While each of the aforementioned designs has its own applicable scenarios, the communication-centric approach is anticipated to be more favorable in future 6G ISAC networks due to its low implementation complexity [9], [10]. This approach allows for the direct use of a communication waveform for sensing, eliminating the need for waveform reshaping. Unlike channel estimation, which only employs known pilot symbols, typical monostatic or cooperative bi-static ISAC systems benefit from the full knowledge of the emitted waveform being shared between the ISAC transmitter (Tx) and the sensing receiver (Rx) [11]. This enables the use of both pilot and data symbols for sensing, thereby enhancing range and Doppler resolutions by fully exploiting time-frequency resources. However, to convey useful information, the communication data symbols have to be *random*, which may degrade the sensing performance. This has been recently identified as a fundamental deterministic-random tradeoff (DRT) in ISAC systems [12], [13]. Consequently, it is essential to seek for optimal communication-centric waveforms that minimize the loss in sensing performance.

Classical communication waveforms convey data symbols using a well-designed orthonormal basis. In its simplest form, such a basis may consist of time-shifted unit impulse functions, corresponding to single-carrier (SC) waveforms [14]. In contrast, OFDM waveforms modulate frequency-domain symbols using multiple sinusoidal subcarriers centered at different frequencies, leveraging the inverse discrete Fourier transform (IDFT) matrix as the signaling basis [9], [15]. Additionally, code-division multiple access (CDMA) schemes use pseudo-random codes, such as Walsh codes constructed

by Hadamard matrices, to carry information symbols [16]. To address the time-frequency doubly selective effect of the high-mobility channels, orthogonal time-frequency space (OTFS) modulation has been proposed as a potential 6G waveform, modulating symbols in the delay-Doppler domain through the inverse symplectic finite Fourier transform (ISFFT) [17], [18]. More recently, a novel affine frequency division multiplexing (AFDM) waveform was conceived for high-mobility communications, which places symbols in the affine Fourier transform (AFT) domains with orthogonal chirp signals as signaling basis [19], [20]. Against this background, an important, yet unresolved question is: *What is the optimal communication-centric ISAC waveform under random signaling?*

A substantial body of work has focused on the analysis and design of communication-centric ISAC waveforms. Pioneered by Sturm and Wiesbeck, the feasibility of using OFDM waveforms to measure delay and Doppler parameters of radar targets has been investigated in [21]. The authors in [22] proposed a code-division OFDM (CD-OFDM) waveform for ISAC, combining CDMA and OFDM techniques. The sensing performance of the cyclic prefixed single-carrier (CP-SC) waveform was examined in [23]. Moreover, the study in [24] demonstrated that OFDM offers superior ranging performance compared to discrete Fourier transform spread OFDM (DFT-s-OFDM), which can be considered as a specific OFDM signaling scheme with SC characteristics. A recent debate has emerged on whether OTFS outperforms OFDM in terms of the sensing performance. The authors in [25] investigated the range and velocity estimation errors of both waveforms, finding that OFDM performs slightly better than OTFS. In [26], the ambiguity functions of both waveforms were illustrated, suggesting that OTFS produces lower sidelobes in both delay and Doppler domains. However, the comparison in [26] was biased, as it utilized random QPSK symbols for OFDM but deterministic symbols for OTFS. More recently, a dual-domain ISAC signaling scheme that integrates both OFDM and OTFS was proposed in [27]. Although existing works have significantly advanced the optimization of communication-centric ISAC waveforms, none has fully addressed the underlying question in a rigorous manner.

In this paper, we attempt to answer this open question from the perspective of target range estimation under a monostatic ISAC setup, where a Tx emits a communication-centric ISAC signal generated by modulating random information symbols over an orthonormal signaling basis. The signal is received by communication users, while being reflected back from distant targets to a sensing Rx collocated with the ISAC Tx. As a consequence, the ISAC signal is fully known to the sensing Rx despite its randomness. The ranging performance is then evaluated by the auto-correlation function (ACF) of the ISAC signal, under both periodic and linear convolutions, corresponding to the matched-filtering operation for signals with and without CP, respectively. For clarity, we summarize our main contributions as follows:

- We developed a generic framework to analyze the sensing performance of communication-centric ISAC waveforms built upon orthonormal signaling basis and random data symbols. Specifically, we analyzed both the P-ACF and

A-ACF of random ISAC signals, and defined the expectation of the integrated sidelobe level (EISL) as a performance metric for ranging.

- We derived closed-form expressions of the sidelobe levels of both the P-ACF and A-ACF for random ISAC signals, under various types of random communication symbols including sub-Gaussian (e.g., QAM and PSK) and super-Gaussian (e.g., specific Amplitude and Phase-Shift Keying (APSK), and index modulation) constellations.
- We proved that among all communication-centric ISAC waveforms with CP, OFDM is the *only* globally optimal waveform that achieves the lowest ranging sidelobe level for standard QAM/PSK constellations, in terms of both EISL and each individual sidelobe index of its P-ACF. As a direct corollary, we also proved that the CP-SC waveform achieves the lowest Doppler sidelobe level.
- We proved that among all communication-centric ISAC waveforms without CP, OFDM is locally optimal in the sense that it achieves a local minimum of the EISL of the A-ACF for QAM/PSK constellations. We also illustrated by simulation that there is no other waveform without CP achieves a lower sidelobe level than that of the OFDM, despite that its global optimality is not guaranteed.

While the superiority of OFDM is well-established in communication systems, its optimality for sensing has not yet been theoretically investigated. We hope this paper would provide theoretical insights into ISAC waveform design under random signaling, and serve as a stepping stone towards the deployment of future 6G ISAC networks.

The remainder of this paper is organized as follows. Sec. II introduces the system model of the considered ISAC system and the corresponding performance metrics. Sec. III and IV elaborate on the periodic and linear ACFs for random ISAC signals and the corresponding optimal signaling strategies, respectively. Sec. V provides simulation results to validate the theoretical analysis of the paper. Finally, Sec. VI concludes the paper.

Notations: Matrices are denoted by bold uppercase letters (e.g., \mathbf{U}), vectors are represented by bold lowercase letters (e.g., \mathbf{x}), and scalars are denoted by normal font (e.g., N); The n th entry of a vector \mathbf{s} , and the (m, n) -th entry of a matrix \mathbf{A} are denoted as s_n and $a_{m,n}$, respectively; \otimes and $\text{vec}(\cdot)$ denote the Kronecker product and the vectorization, $(\cdot)^T$, $(\cdot)^H$, and $(\cdot)^*$ stand for transpose, Hermitian transpose, and complex conjugate of the matrices; $\text{Re}(\cdot)$ and $\text{Im}(\cdot)$ denote the real and imaginary parts of the argument; l_p norm and the Frobenius norm are written as $\|\cdot\|_p$ and $\|\cdot\|_F$, and $\mathbb{E}(\cdot)$ represents the expectation operation. The symbol $\delta_{m,n}$ denotes the Kronecker delta function given by

$$\delta_{m,n} = \begin{cases} 0, & m \neq n; \\ 1, & m = n. \end{cases}$$

II. SYSTEM MODEL

A. ISAC Signal Model

We consider a monostatic ISAC system as shown in Fig. 1. The ISAC Tx emits an ISAC signal modulated with random

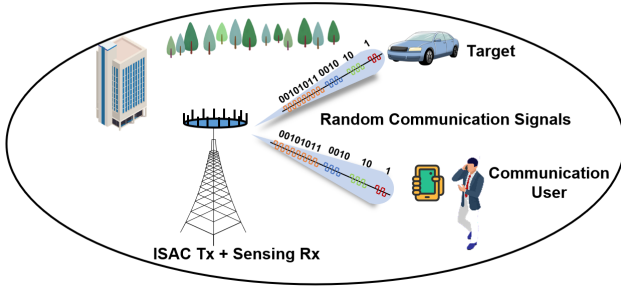


Fig. 1. The ISAC transmission scenario using communication-centric waveform.

communication symbols, which is received at a communication Rx, and is simultaneously reflected back to the sensing Rx by one or more targets at different ranges. The sensing Rx, which is collocated with the ISAC Tx, performs matched-filtering to estimate the delay parameters of targets by using the known random ISAC signal.

Let $\mathbf{s} = [s_1, s_2, \dots, s_N]^T \in \mathbb{C}^{N \times 1}$ be N communication symbols to be transmitted. We assume that each symbol is randomly drawn from a complex alphabet in an i.i.d. manner, which is also known as a *constellation*. Without loss of generality, we adopt the following assumptions for the considered constellations.

Assumption 1 (Unit Power). *We focus on constellations with a unit power, namely,*

$$\mathbb{E}(|s_n|^2) = 1, \quad \forall n. \quad (1)$$

Assumption 1 normalizes the power of the constellations such that their sensing and communication performance could be fairly compared.

Assumption 2 (Rotational Symmetry). *The expectation and pseudo variance of the constellation are zero, namely*

$$\mathbb{E}(s_n) = 0, \quad \mathbb{E}(s_n^2) = 0, \quad \forall n. \quad (2)$$

We remark that most of the commonly employed constellations meet the criterion in Assumption 2, including all the PSK and QAM constellations except for BPSK and 8-QAM. Nevertheless, we will show in later sections that our results are indeed applicable to BPSK, which makes 8-QAM the only outlier of the proposed framework.

Let us further define

$$\mu_4 \triangleq \frac{\mathbb{E}\{|s_n - \mathbb{E}(s_n)|^4\}}{\mathbb{E}\{|s_n - \mathbb{E}(s_n)|^2\}^2} = \mathbb{E}(|s_n|^4), \quad (3)$$

which is known as the *kurtosis* of the constellation, and is equivalent to its 4th-order moment if the constellation has zero mean and unit power. Note that $\mu_4 \geq 1$ since the 4th-moment is greater than the square of the 2nd-moment.

It is worth highlighting that the standard complex Gaussian distribution also satisfies the above criteria, which makes it an adequate constellation. Indeed, it is well-known that the Gaussian distributed constellation achieves the capacity of a Gaussian channel. As we shall see later, the standard complex Gaussian constellation, which has a kurtosis of 2, also serves

TABLE I
KURTOSIS VALUES OF TYPICAL SUB-GAUSSIAN CONSTELLATIONS

Constellation	PSK	16-QAM	64-QAM	128-QAM
Kurtosis	1	1.32	1.381	1.3427
Constellation	256-QAM	512-QAM	1024-QAM	2048-QAM
Kurtosis	1.3953	1.3506	1.3988	1.3525

as an important baseline in terms of the sensing performance of the ISAC signal. Accordingly, it would be useful to define the following two types of constellations.

Definition 1 (Sub-Gaussian Constellation). *A sub-Gaussian constellation is a constellation with kurtosis less than 2, subject to Assumptions 1 and 2.*

Definition 2 (Super-Gaussian Constellation). *A super-Gaussian constellation is a constellation with kurtosis greater than 2, subject to Assumptions 1 and 2.*

All the QAM and PSK constellations are sub-Gaussian. In particular, the kurtosis is equal to 1 for all PSK constellations, and is between 1 and 2 for all QAM constellations. For clarity, we show the kurtosis values of typical QAM and PSK constellations in TABLE I. There are certain types of super-Gaussian constellations with drastically varying amplitudes. Alternatively, one may also generate super-Gaussian constellations by applying geometric or probabilistic constellation shaping techniques. Index modulation (IM) [28], [29] is one of such techniques that are capable of producing super-Gaussian constellations. To elaborate, let us consider a constellation having a kurtosis of μ_4 . By applying the IM, a probability mass would be placed at the origin of the I/Q plane, while leaving the rest of the constellation unaltered. Assuming that the probability of transmitting the origin is p_0 , the resulting kurtosis would then become

$$\tilde{\mu}_4 = \frac{(1-p_0)\mathbb{E}\{|s_n - \mathbb{E}(s_n)|^4\}}{\mathbb{E}\{(1-p_0)|s_n - \mathbb{E}(s_n)|^2\}^2} = \frac{\mu_4}{1-p_0} \geq \frac{1}{1-p_0}. \quad (4)$$

Observe that having an origin-transmitting probability of $p_0 > \frac{1}{2}$ would effectively transform any constellation into a super-Gaussian one. Super-Gaussian constellations can be useful in scenarios where energy efficiency is of priority or non-coherent communication schemes are considered [30]–[32].

In typical communication systems, we shall modulate N symbols over an orthonormal basis on the time domain, which may be defined as a unitary matrix $\mathbf{U} = [\mathbf{u}_1, \mathbf{u}_2, \dots, \mathbf{u}_N] \in \mathbb{U}(N)$, where $\mathbb{U}(N)$ denotes the unitary group of degree N . Consequently, the discrete time-domain signal can be expressed as

$$\mathbf{x} = \mathbf{U}\mathbf{s} = \sum_{n=1}^N s_n \mathbf{u}_n. \quad (5)$$

The above generic model may represent most of the communication signaling schemes, where we show some examples below:

- **SC Waveform:** $\mathbf{U} = \mathbf{I}_N$. In this case, we are simply transmitting symbols consecutively on the time domain, where the orthonormal basis is composed of nothing but unit impulse functions, yielding an SC signal.

- **OFDM:** $\mathbf{U} = \mathbf{F}_N^H$, where \mathbf{F}_N is the normalized discrete Fourier transform (DFT) matrix of size N . The symbols are placed in the frequency domain, which makes \mathbf{x} an OFDM signal with N subcarriers. If L OFDM symbols are transmitted with $M = N/L$ subcarriers, then $\mathbf{U} = \mathbf{I}_L \otimes \mathbf{F}_M^H$.
- **CDMA:** $\mathbf{U} = \mathbf{C}_N$, where \mathbf{C}_N is the Hadamard matrix of size N . The symbols are then placed in the code domain, making \mathbf{x} a CDMA signal that has been extensively used in CDMA2000 [33].
- **OTFS:** $\mathbf{U} = \mathbf{F}_M^H \otimes \mathbf{I}_L$. In this case, \mathbf{s} is placed in the delay-Doppler domain, where the number of occupied time slots and subcarriers are L and M , respectively [34].
- **AFDM:** $\mathbf{U} = \Lambda_{c_1}^H \mathbf{F}_N^H \Lambda_{c_2}^H$ [19], [20], where $\Lambda_c = \text{Diag}(1, e^{-j2\pi c1^2}, \dots, e^{-j2\pi cN^2})$. In this case, \mathbf{U} is the inverse discrete affine Fourier transform (IDAFST) matrix, and the symbols are placed in the AFT domain.

We highlight here that in many communication signaling schemes, such as OFDM, CP-SC (also known as single-carrier frequency-domain equalization (SC-FDE)) [35], OTFS, and AFDM, the addition of a cyclic prefix (CP) is necessary, which eliminates the inter-symbol interference (ISI) and reduces the computational complexity by processing the received signal in the frequency/delay-Doppler domain. Nevertheless, adding CPs to the signal may not always be a convention in radar sensing systems. This is because for long-range detection tasks, the targets may be located far beyond the coverage of a CP, in which case a sufficiently small duty cycle ($< 10\%$) is required, rendering the ISAC signal as a zero-padding waveform in contrast to its CP'ed counterpart.

Towards that end, we present in this paper a thorough analysis on both cases, i.e., ISAC signaling with and without CP, which correspond to periodic and linear convolution processing of the matched-filter at the sensing Rx, respectively. Without loss of the generality, whenever a CP is added, it is assumed to be larger than the maximum delay of the communication paths and sensing targets.

B. Communication System Model

Before delving into the technical details, let us first briefly examine the communication performance of the ISAC signal under two typical communication channels: The additive white Gaussian noise (AWGN) channel and linear time-invariant (LTI) multi-path channel, where we assume a CP is added to the signal for the purpose stated above. In the AWGN case, the received signal after CP removal reads

$$\mathbf{y}_c = \sqrt{\rho}\mathbf{x} + \mathbf{z} = \sqrt{\rho}\mathbf{U}\mathbf{s} + \mathbf{z}, \quad (6)$$

where ρ is the signal-to-noise ratio (SNR), and $\mathbf{z} \sim \mathcal{CN}(\mathbf{0}, \mathbf{I}_N)$ denotes the WGN with zero mean and unit variance. It then holds immediately that

$$I(\mathbf{y}_c; \mathbf{x}) = I(\sqrt{\rho}\mathbf{U}\mathbf{s} + \mathbf{z}; \mathbf{U}\mathbf{s}) = I(\mathbf{y}_c; \mathbf{s}). \quad (7)$$

That is, unitary transform keeps the input-output mutual information (MI) unchanged in an AWGN channel, thereby preserving the communication achievable rate. More precisely, in an AWGN channel, the communication symbols may be

modulated over arbitrary orthonormal basis, without performance loss in the communication rate.

Let us now turn our focus to the LTI multi-path channel with WGN, which outputs the following signal at the communication Rx after removing the CP:

$$\mathbf{y}_c = \sqrt{\rho}\mathbf{H}_c\mathbf{x} + \mathbf{z} = \sqrt{\rho}\mathbf{H}_c\mathbf{U}\mathbf{s} + \mathbf{z}, \quad (8)$$

where \mathbf{H}_c is a circulant matrix, with each row containing circularly ordered entries, namely the complex channel gains at multiple delayed paths. In such a channel, the MI is no longer invariant under unitary transform [36]. Let us consider two signaling bases $\mathbf{U} \neq \mathbf{U}'$. It generally holds that

$$I(\sqrt{\rho}\mathbf{H}_c\mathbf{U}\mathbf{s} + \mathbf{z}; \mathbf{U}\mathbf{s}) \neq I(\sqrt{\rho}\mathbf{H}_c\mathbf{U}'\mathbf{s} + \mathbf{z}; \mathbf{U}'\mathbf{s}) \quad (9)$$

which suggests that the choice of signaling basis indeed affects the communication performance. To achieve the capacity of the LTI multi-path channel, as well as to reduce the symbol detection complexity, it is well-recognized that \mathbf{H}_c shall be diagonalizable by \mathbf{U} , where a possible option is the IDFT matrix given the circularity of \mathbf{H}_c , leading to $\mathbf{U} = \mathbf{F}_N^H$. By doing so, and performing DFT to the received signal, we obtain

$$\mathbf{F}_N\mathbf{y}_c = \mathbf{F}_N\mathbf{H}_c\mathbf{F}_N^H\mathbf{s} + \mathbf{F}_N\mathbf{z} = \mathbf{\Sigma}\mathbf{s} + \mathbf{F}_N\mathbf{z}, \quad (10)$$

where $\mathbf{\Sigma}$ is a diagonal matrix containing the frequency-domain channel coefficients, and $\mathbf{F}_N\mathbf{z} \sim \mathcal{CN}(\mathbf{0}, \mathbf{I}_N)$ is identically distributed with \mathbf{z} .

The above analysis confirms the superiority of leveraging the OFDM signaling in an LTI multi-path communication channel. One would then wonder whether the OFDM is still optimal for sensing, especially under random ISAC signaling. This represents a long-standing open question in the area of ISAC: What is the optimal communication-centric ISAC waveform? In later sections, we attempt to answer this question by rigorously proving that the OFDM is the optimal waveform that achieves the lowest ranging sidelobe under QAM/PSK alphabets.

C. Sensing Performance Metric

The auto-correlation function (ACF) of the signal is an important performance indicator for ranging, in particular for the matched filtering process at the sensing Rx. The ACF may be defined as the linear or periodic self-convolution of the signal, depending on whether a CP is added to the signal.

1) Aperiodic ACF (A-ACF):

$$r_k = \mathbf{x}^H \mathbf{J}_k \mathbf{x} = r_{-k}^*, \quad k = 0, 1, \dots, N-1, \quad (11)$$

where \mathbf{J}_k is the k th shift matrix in the form of

$$\mathbf{J}_k = \begin{bmatrix} \mathbf{0} & \mathbf{I}_{N-k} \\ \mathbf{0} & \mathbf{0} \end{bmatrix}. \quad (12)$$

Given the symmetry of the ACF, we have

$$\mathbf{J}_{-k} = \mathbf{J}_k^T = \begin{bmatrix} \mathbf{0} & \mathbf{0} \\ \mathbf{I}_{N-k} & \mathbf{0} \end{bmatrix}. \quad (13)$$

2) *Periodic ACF (P-ACF)*:

$$\tilde{r}_k = \mathbf{x}^H \tilde{\mathbf{J}}_k \mathbf{x} = \tilde{r}_{-k}^*, \quad k = 0, 1, \dots, N-1, \quad (14)$$

where $\tilde{\mathbf{J}}_k$ is defined as the k th periodic shift matrix [37], given as

$$\tilde{\mathbf{J}}_k = \begin{bmatrix} \mathbf{0} & \mathbf{I}_{N-k} \\ \mathbf{I}_k & \mathbf{0} \end{bmatrix}, \quad (15)$$

and

$$\tilde{\mathbf{J}}_{-k} = \tilde{\mathbf{J}}_k^T = \begin{bmatrix} \mathbf{0} & \mathbf{I}_k \\ \mathbf{I}_{N-k} & \mathbf{0} \end{bmatrix}. \quad (16)$$

In both cases, one may be concerned by the sidelobe level of the ACF, which plays a critical role in multi-target detection problems. Let us take the A-ACF as an example. The sidelobe of r_k is defined as

$$|r_k|^2 = |\mathbf{x}^H \mathbf{J}_k \mathbf{x}|^2 = |r_{-k}|^2, \quad k = 1, \dots, N-1, \quad (17)$$

where $|r_0|^2 = |\mathbf{x}^H \mathbf{x}|^2 = \|\mathbf{x}\|_2^4$ is the mainlobe of the ACF. Accordingly, the integrated sidelobe level (ISL) may be expressed as [38], [39]

$$\text{ISL} = \sum_{k=1}^{N-1} |r_k|^2. \quad (18)$$

Due to the random nature of the ISAC signal \mathbf{x} , the ACF becomes a random function. We are therefore tempted to define the average of the sidelobe level as a performance metric. This can be represented by

$$\mathbb{E}(|r_k|^2) = \mathbb{E}(|\mathbf{x}^H \mathbf{J}_k \mathbf{x}|^2) = \mathbb{E}(|\mathbf{s}^H \mathbf{U}^H \mathbf{J}_k \mathbf{U} \mathbf{s}|^2), \quad \forall k, \quad (19)$$

where the expectation is with respect to the random symbol vector \mathbf{s} , $\mathbb{E}(|r_0|^2) = \mathbb{E}(\|\mathbf{x}\|_2^4)$ denotes the average mainlobe, and $\mathbb{E}(|r_k|^2), k \neq 0$ characterizes the average sidelobe level at the index k . The expectation of the ISL (EISL) is therefore given by

$$\text{EISL} = \sum_{k=1}^{N-1} \mathbb{E}(|r_k|^2) = \sum_{k=1}^{N-1} \mathbb{E}(|\mathbf{s}^H \mathbf{U}^H \mathbf{J}_k \mathbf{U} \mathbf{s}|^2). \quad (20)$$

Accordingly, seeking for the optimal signaling basis is equivalent to solving the following stochastic optimization problem:

$$\min_{\mathbf{U} \in \mathbb{U}(N)} \sum_{k=1}^{N-1} \mathbb{E}(|\mathbf{s}^H \mathbf{U}^H \mathbf{J}_k \mathbf{U} \mathbf{s}|^2). \quad (21)$$

Remark 1: It is worth pointing out that if \mathbf{s} is realized from a Gaussian codebook, namely, $s_n \sim \mathcal{CN}(0, 1)$, then the average mainlobe and sidelobe levels of its ACFs will keep unchanged regardless of the choice of the signaling basis. This is due to the simple fact that the standard Gaussian distribution is unitary invariant.

While attaining the analytical solution of (21) for an arbitrarily distributed constellation seems to be a highly challenging task, in what follows, we reveal that the OFDM waveform achieves the lowest ranging sidelobe for both QAM and PSK. That is to say, $\mathbf{U} = \mathbf{F}_N^H$ is a minimizer of the EISL for both the A-ACF and P-ACF when \mathbf{s} is realized from QAM/PSK constellations. We will further prove that, OFDM is the only globally optimal waveform that minimizes not only the EISL but also the individual sidelobe level at each $k \neq 0$ in the P-ACF case.

III. THE P-ACF CASE

Although being similarly formulated, dealing with the P-ACF is generally a simpler task than its aperiodic counterpart. In this section, we present the main results of the P-ACF case. Let us first demonstrate the basic structure of the periodic shift matrix in Lemma 1.

Lemma 1. *The periodic shift matrix can be decomposed as*

$$\tilde{\mathbf{J}}_k = \sqrt{N} \mathbf{F}_N^H \text{Diag}(\mathbf{f}_{N-k+1}) \mathbf{F}_N, \quad (22)$$

where \mathbf{f}_k is the k th column of \mathbf{F}_N .

By leveraging Lemma 1, we may simplify the P-ACF by exploiting the frequency-domain representation of the ISAC signal. By performing DFT to \mathbf{x} , we obtain

$$\mathbf{F}_N \mathbf{x} = \mathbf{F}_N \mathbf{U} \mathbf{s} \triangleq \mathbf{V}^H \mathbf{s}, \quad (23)$$

where $\mathbf{V} = \mathbf{U}^H \mathbf{F}_N^H = [\mathbf{v}_1, \mathbf{v}_2, \dots, \mathbf{v}_N] \in \mathbb{U}(N)$. Accordingly, the P-ACF may be recast as

$$\begin{aligned} \tilde{r}_k &= \mathbf{x}^H \tilde{\mathbf{J}}_k \mathbf{x} = \sqrt{N} \mathbf{s}^H \mathbf{V} \text{Diag}(\mathbf{f}_{N-k+1}) \mathbf{V}^H \mathbf{s} \\ &= \sum_{n=1}^N |\mathbf{v}_n^H \mathbf{s}|^2 e^{-\frac{j2\pi(N-k)(n-1)}{N}} = \sum_{n=1}^N |\mathbf{v}_n^H \mathbf{s}|^2 e^{\frac{j2\pi k(n-1)}{N}}, \quad \forall k, \end{aligned} \quad (24)$$

which is the IDFT of the sequence $|\mathbf{v}_n^H \mathbf{s}|^2$ up to a factor $\frac{1}{N}$. To proceed, we introduce another useful lemma below.

Lemma 2. *Let $\tilde{\mathbf{s}} = \text{vec}(\mathbf{s}\mathbf{s}^H)$. For constellations that meet the Assumptions 1 and 2, we have*

$$\begin{aligned} \mathbf{S} &= \mathbb{E}(\tilde{\mathbf{s}}\tilde{\mathbf{s}}^H) \\ &= \begin{bmatrix} \mu_4 & \mathbf{0}_N^T & 1 & \mathbf{0}_N^T & 1 & \dots & 1 \\ \mathbf{0}_N & \mathbf{I}_N & \mathbf{0}_N & \mathbf{0}_N & \mathbf{0}_N & \dots & \mathbf{0}_N \\ 1 & 0 & \mu_4 & \dots & 1 & \dots & 1 \\ \mathbf{0}_N & \mathbf{0}_N & \mathbf{0}_N & \mathbf{I}_N & \vdots & \dots & \vdots \\ 1 & 0 & 1 & 0 & \mu_4 & \dots & 1 \\ \vdots & \vdots & \vdots & \vdots & \vdots & \ddots & \mathbf{0}_N \\ 1 & 0 & 1 & 0 & 1 & \dots & \mu_4 \end{bmatrix} \in \mathbb{R}^{N^2 \times N^2}, \end{aligned} \quad (25)$$

where μ_4 is the kurtosis of the constellation, and $\mathbf{0}_N$ represents the all-zero vector with length N .

Proof. See Appendix A. ■

A. Main Results

With Lemmas 1 and 2 at hand, we are now ready to express the squared P-ACF in closed form.

Proposition 1. *The average squared P-ACF is*

$$\mathbb{E}(|\tilde{r}_k|^2) = N^2 \delta_{0,k} + N + (\mu_4 - 2) \|\mathbf{b}_k\|_2^2, \quad (26)$$

where

$$\mathbf{b}_k = \left[\sum_{n=1}^N |v_{1,n}|^2 e^{-\frac{j2\pi k(n-1)}{N}}, \dots, \sum_{n=1}^N |v_{N,n}|^2 e^{-\frac{j2\pi k(n-1)}{N}} \right]^T, \quad (27)$$

with $v_{m,n}$ being the (m, n) -th entry of \mathbf{V} .

Proof. See Appendix B

Corollary 1. *The average mainlobe level of the P-ACF may be expressed as*

$$\mathbb{E}(|\tilde{r}_0|^2) = N^2 + (\mu_4 - 1)N. \quad (28)$$

Proof. It can be readily shown that $\mathbf{b}_0 = \mathbf{1}_N$, and hence $\|\mathbf{b}_0\|_2^2 = N$, which immediately yields (28). ■

Proposition 2. *The EISL of the P-ACF is*

$$\sum_{k=1}^{N-1} \mathbb{E}(|\tilde{r}_k|^2) = N(N-1) + (\mu_4 - 2)N(\|\mathbf{F}_N \mathbf{U}\|_4^4 - 1), \quad (29)$$

where $\|\cdot\|_4$ denotes the ℓ_4 norm of the matrix.

Proof. See Appendix C. ■

B. Optimal Signaling Schemes

We may now establish the optimality of the OFDM waveform in Theorem 1.

Theorem 1 (Global Optimality of the OFDM for Ranging). *OFDM is the only waveform that achieves the lowest EISL of the P-ACF for sub-Gaussian constellations, e.g., PSK and QAM.*

Proof. To minimize the EISL in the $\mu_4 < 2$ case, it is obvious from Proposition 2 that one has to maximize $\|\mathbf{F}_N \mathbf{U}\|_4^4$ over the unitary group, i.e.,

$$\max_{\mathbf{U} \in \mathbf{U}(N)} \|\mathbf{F}_N \mathbf{U}\|_4^4. \quad (30)$$

All the global maximizers of the ℓ_4 norm are known to belong to the set of *complex permutation* matrices [40], which is defined as the product of a real permutation matrix and any diagonal unitary matrix. Consequently, the optimal signaling basis shall be expressed in the form of

$$\mathbf{U}^* = \mathbf{F}_N^H \mathbf{\Pi} \text{Diag}(\boldsymbol{\theta}), \quad (31)$$

where $\mathbf{\Pi} \in \mathbb{R}^{N \times N}$ is any real permutation matrix, and $\boldsymbol{\theta} \in \mathbb{C}^N$ is a vector with unit-modulus entries. If $\mathbf{\Pi} = \mathbf{I}_N$, $\boldsymbol{\theta} = \mathbf{1}_N$, then \mathbf{U}^* represents the standard OFDM waveform. Otherwise, (31) simply results in an OFDM waveform with different initial phases over permuted subcarriers, completing the proof. ■

From Theorem 1 it is obvious that for $\mu_4 < 2$ we have

$$\sum_{k=1}^{N-1} \mathbb{E}(|r_k|^2) \geq (\mu_4 - 1)N(N-1), \quad (32)$$

since $\|\mathbf{F}_N \mathbf{U}^*\|_4^4 = N$. Furthermore, the following theorem provides a stronger result for the optimality of the OFDM.

Theorem 2 (OFDM Achieves the Lowest Sidelobe at Every Lag). *OFDM is the only waveform that achieves the lowest sidelobe level at every delay index k of the P-ACF for sub-Gaussian constellations.*

■ *Proof.* We first establish an upper-bound for $\|\mathbf{b}_k\|_2^2$, and then prove that it is achievable by the OFDM waveform. Given the fact that $\mu_4 \geq 1$, for $k \neq 0$ we have

$$\mathbb{E}(|\tilde{r}_k|^2) = N + (\mu_4 - 2) \|\mathbf{b}_k\|_2^2 \geq N - \|\mathbf{b}_k\|_2^2 \geq 0, \quad (33)$$

which suggests that $\|\mathbf{b}_k\|_2^2 \leq N$ at every sidelobe index k . Now suppose that the OFDM is employed as the signaling basis, then the optimal \mathbf{V} may be expressed as

$$\mathbf{V}^* = \mathbf{U}^{*H} \mathbf{F}_N^H = \text{Diag}(\boldsymbol{\theta}) \mathbf{\Pi}, \quad (34)$$

in which case we have

$$\|\mathbf{v}_n \odot \mathbf{v}_m\|_2^2 = \delta_{n,m}, \quad (35)$$

owing to the structure of the permutation matrix $\mathbf{\Pi}$. As a consequence, we have $\|\mathbf{b}_k\|_2^2 = N$ as per (62). This suggests that $\|\mathbf{b}_k\|_2^2 \leq N$ is a supremum for every $k \neq 0$, and that

$$\mathbb{E}(|\tilde{r}_k|^2) \geq (\mu_4 - 1)N, \quad \forall k \neq 0, \quad (36)$$

is an infimum of each individual sidelobe, both of which are achieved by the OFDM basis (31). This indicates that OFDM achieves the lowest sidelobe level at every lag.

We may now prove the uniqueness of the OFDM as a global minimizer of every ranging sidelobe by contradiction. Suppose that there exists another signaling basis matrix \mathbf{U}' that achieves the infimum in (36), but has a different form from (31). Then it holds immediately that \mathbf{U}' also minimizes the EISL. This contradicts Theorem 1, which states that OFDM is the only EISL minimizer, completing the proof. ■

Remark 2: An interesting, but not surprising fact is that for PSK constellations ($\mu_4 = 1$), both the individual and integrated sidelobe levels are zero under OFDM signaling, which means that the P-ACF of OFDM-PSK signal is always a unit impulse function. This attribute has nothing to do with the randomness of the PSK, as it can be simply deduced from (24) by letting $\mathbf{V} = \mathbf{I}_N$ for any realization of PSK sequences, which originates from the duality of Fourier transform (FT), that the FT of a unit impulse function is a constant over all frequencies. However, as we shall see later, this does not hold for the A-ACF case, where PSK constellations always generate non-zero sidelobes.

Corollary 2 (Optimality of the CP-SC for Doppler Measurement). *CP-SC is the only waveform that achieves the lowest Doppler sidelobe level for sub-Gaussian constellations in the P-ACF case.*

Proof. We highlight that the Doppler sidelobe is generated from the ACF of the frequency spectrum of the signal, which is also known as the zero-delay slice of the ambiguity function. In the periodic convolution case, this can be expressed as

$$\tilde{g}_k = \mathbf{x}^H \mathbf{F}_N^H \tilde{\mathbf{J}}_k \mathbf{F}_N \mathbf{x} = \mathbf{s}^H \mathbf{U}^H \mathbf{F}_N^H \tilde{\mathbf{J}}_k \mathbf{F}_N \mathbf{U} \mathbf{s}, \quad (37)$$

where $\mathbf{F}_N \mathbf{x}$ is the frequency-domain signal. Based on Theorems 1 and 2, in order to minimize the sidelobe level of $\mathbb{E}(|\tilde{g}_k|^2)$, the globally optimal \mathbf{U} should have the following structure:

$$\mathbf{U}^\dagger = \mathbf{F}_N^H \mathbf{F}_N^H \mathbf{\Pi} \text{Diag}(\boldsymbol{\theta}). \quad (38)$$

Note that $\mathbf{F}_N^H \mathbf{F}_N^H$ is a permutation matrix in the form of

$$\mathbf{F}_N^H \mathbf{F}_N^H = \begin{bmatrix} 1 & 0 & \cdots & 0 \\ 0 & 0 & \cdots & 1 \\ \vdots & \vdots & \ddots & \vdots \\ 0 & 1 & \cdots & 0 \end{bmatrix}. \quad (39)$$

Accordingly, simply by letting $\mathbf{\Pi}$ take the same form of (39), and $\boldsymbol{\theta} = \mathbf{1}_N$, we have

$$\mathbf{U}^\dagger = \mathbf{I}_N, \quad (40)$$

which suggests that $\mathbf{x} = \mathbf{U}^\dagger \mathbf{s} = \mathbf{s}$ is an SC waveform with CP. Otherwise, if $\mathbf{\Pi}$ and $\boldsymbol{\theta}$ take other possible forms, then \mathbf{x} is still an CP-SC waveform subject to permutation and different initial phases over N time-domain symbols. This completes the proof. ■

We now investigate the ranging performance of the $\mu_4 > 2$ case, i.e., when \mathbf{s} is randomly realized from a super-Gaussian constellation.

Corollary 3. *CP-SC achieves the lowest EISL for super-Gaussian constellations in the P-ACF case.*

Proof. Let us recall (29). To minimize the EISL in the $\mu_4 > 2$ case, one needs to minimize $\|\mathbf{F}_N \mathbf{U}\|_4^4$ over the unitary group. Note that under a fixed l_2 norm, the l_4 norm is minimized if each entry has a constant modulus, which suggests that $\mathbf{U} = \mathbf{I}_N$ is a minimizer. This completes the proof. ■

Remark 3: It is also interesting to point out that when $\mathbf{U} = \mathbf{I}_N$, we have $\|\mathbf{F}_N \mathbf{U}\|_4^4 = 1$ and $\|\mathbf{b}_k\|^2 = 0$ for $k \neq 0$. This implies that using CP-SC signaling results in a ranging EISL of $N(N-1)$, and a uniform sidelobe level $\mathbb{E}(|\tilde{r}_k|^2) = N$ at each index $k \neq 0$, no matter what value that μ_4 takes. Moreover, we see that the Gaussian constellation with $\mu_4 = 2$ produces exactly the same EISL and individual sidelobe level regardless of the choice of \mathbf{U} , which is consistent with its unitary invariance property. This observation suggests that under the CP-SC signaling, all the constellations behave like Gaussian in terms of ranging. In such a case, the only difference lies in their mainlobe levels, where the super-Gaussian constellation may slightly outperform other constellations, since a larger kurtosis yields higher mainlobe as per (28).

IV. THE A-ACF CASE

In this section, we analyze the ranging performance of random ISAC signals by investigating the sidelobe levels of the A-ACF.

A. Main Results

Proposition 3. *The average squared A-ACF is*

$$\mathbb{E}(|r_k|^2) = N^2 \delta_{0,k} + N - k + (\mu_4 - 2) \sum_{n=1}^N |\mathbf{u}_n^H \mathbf{J}_k \mathbf{u}_n|^2. \quad (41)$$

Proof. See Appendix D. ■

Note that the average mainlobe level of the A-ACF stays the same with that of the P-ACF as in Corollary 1. To proceed, we analyze the EISL of the A-ACF in Proposition 4.

Proposition 4. *The EISL of the A-ACF is*

$$\sum_{k=1}^{N-1} \mathbb{E}(|r_k|^2) = \frac{N(N-1)}{2} + (\mu_4 - 2)N \left(\|\tilde{\mathbf{F}}_{2N} \mathbf{U}\|_4^4 - \frac{1}{2} \right), \quad (42)$$

where $\tilde{\mathbf{F}}_{2N} \in \mathbb{C}^{2N \times N}$ contains the first N columns of the size- $2N$ DFT matrix \mathbf{F}_{2N} .

Proof. See Appendix E. ■

B. Optimal Signaling Schemes

In order to minimize the EISL for sub-Gaussian constellations ($\mu_4 < 2$), one has to solve the following l_4 norm maximization problem:

$$\max_{\mathbf{U} \in \mathbb{U}(N)} \|\tilde{\mathbf{F}}_{2N} \mathbf{U}\|_4^4. \quad (43)$$

Unfortunately, solving (43) is much more difficult than solving its counterpart (30), since it is not possible to produce a complex permutation matrix through multiplying $\tilde{\mathbf{F}}_{2N}$ with a size- N unitary matrix. While substituting the size- N IDFT matrix indeed yields a large objective value, we do not know whether it is a globally optimal solution. In fact, maximizing the l_4 norm $\|\mathbf{Z}\mathbf{U}\|_4$ over the unitary group for arbitrary \mathbf{Z} generally remains an open problem [41]. Towards that end, we seek to provide a local maximum of (43) by relying on a Coordinate Ascent (CA) algorithm over $\mathbb{U}(N)$. The CA algorithm for l_4 norm maximization was originally proposed in [40] when \mathbf{Z} is a row vector. In this paper, we generalize it to the matrix version. On top of that, we establish the local optimality of the IDFT matrix for problem (43), which in turn offers theoretical guarantee for the optimality of the OFDM signaling in the A-ACF case.

The CA algorithm relies on the fact that unitary matrices can be parameterized as a product of real-valued Givens rotation matrices and complex-valued phase shift matrices. A Givens rotation matrix $\mathbf{G}_{l,k}(\alpha) \in \mathbb{C}^{N \times N}$ is defined as [42]

$$\mathbf{G}_{l,k}(\alpha) = \begin{bmatrix} \mathbf{I}_{l-1} & 0 & 0 \cdots & 0 & 0 \\ 0 & \cos(\alpha) & 0 \cdots & \sin(\alpha) & \vdots \\ \vdots & 0 & \mathbf{I}_{k-l-1} & 0 \cdots & 0 \\ 0 & -\sin(\alpha) & \vdots & \cos(\alpha) & 0 \\ 0 & 0 & \cdots & 0 & \mathbf{I}_{N-k} \end{bmatrix}, \quad (44)$$

where $k > l$. Note that left-multiplying $\mathbf{G}_{l,k}(\alpha)$ to a matrix indicates a counter-clockwise rotation of an angle α in the (l, k) coordinate plane. Moreover, the phase rotation matrix $\mathbf{R}_k(\beta) \in \mathbb{C}^{N \times N}$ is defined as the following diagonal matrix:

$$\mathbf{R}_k(\beta) = \begin{bmatrix} \mathbf{I}_{k-1} & 0 \cdots & 0 \\ 0 \cdots & e^{j\beta} & \vdots \\ 0 \cdots & 0 \cdots & \mathbf{I}_{N-k} \end{bmatrix}. \quad (45)$$

By observing the fact that the multiplication of $\mathbf{G}_{l,k}(\alpha)$ and $\mathbf{R}_k(\beta)$ preserves the unitarity, we may maximize (43) in

Algorithm 1 CA Algorithm for Solving (43)

Input: $\varepsilon > 0$, and the maximum iteration number t_{\max}
Output: \mathbf{U}^*

 1. Initialize $\mathbf{U}_0 \in \mathbb{U}(N)$.

while $t \leq t_{\max}$ and $\|\mathbf{U}_{t+1} - \mathbf{U}_t\|_F^2 \geq \varepsilon$ **do**

 2. Update $\alpha_{l,k}$ by

$$\alpha_{l,k} = \arg \max_{\alpha \in [0, \pi/2)} \left\| \mathbf{G}_{k,l}(\alpha) \mathbf{U}_t^H \tilde{\mathbf{F}}_{2N}^H \right\|_4^4.$$

 3. Update β_l and β_k by

$$\begin{aligned} & \{\beta_l, \beta_k\} \\ &= \arg \max_{\{\theta, \phi\} \in [0, 2\pi)} \left\| \mathbf{G}_{k,l}(\alpha_{l,k}) \mathbf{R}_l(\theta) \mathbf{R}_k(\phi) \mathbf{U}_t^H \tilde{\mathbf{F}}_{2N}^H \right\|_4^4. \end{aligned}$$

 4. Update \mathbf{U}_{t+1} by

$$\mathbf{U}_{t+1} = \mathbf{U}_t \mathbf{R}_k(-\beta_k) \mathbf{R}_l(-\beta_l) \mathbf{G}_{l,k}(-\alpha_{l,k}).$$

 5. $t = t + 1$.

end while

an iterative manner by maximizing over α and β at each (l, k) index, which corresponds to Algorithm 1. Note that each update of α and β may be simply attained via a one-dimensional search.

It is provable that Algorithm 1 yields a local maximum of (43). Under such a framework, we may prove the local optimality of the IDFT solution $\mathbf{U}^* = \mathbf{F}_N^H$ through [40, Lemma 3], which follows from the first- and second-derivative tests, and is recalled as below.

Lemma 3. *Let $\mathbf{D} = \mathbf{U}^H \tilde{\mathbf{F}}_{2N}^H$. Then \mathbf{U} is a local maximum of (43) if and only if the following two conditions hold for all $k > l$:*

$$\begin{aligned} & \left. \frac{\partial \|\mathbf{G}_{l,k}(\alpha) \mathbf{D}\|_4^4}{\partial \alpha} \right|_{\alpha=0} \\ &= 4 \sum_{m=1}^{2N} \left(|d_{l,m}|^2 - |d_{k,m}|^2 \right) \operatorname{Re} (d_{l,m}^* d_{k,m}) = 0, \quad (46) \end{aligned}$$

$$\begin{aligned} & \left. \frac{\partial^2 \|\mathbf{G}_{l,k}(\alpha) \mathbf{D}\|_4^4}{\partial \alpha^2} \right|_{\alpha=0} = 4 \sum_{m=1}^{2N} 2 \operatorname{Re} (d_{k,m}^2 d_{l,m}^{*2}) \\ & + 4 |d_{l,m}|^2 |d_{k,m}|^2 - |d_{l,m}|^4 - |d_{k,m}|^4 < 0, \quad (47) \end{aligned}$$

where $d_{k,m}$ is the (k, m) -th entry of \mathbf{D} .

Proof. See [40]. ■

The local optimality of the OFDM signaling holds immediately by substituting $\mathbf{U}^* = \mathbf{F}_N^H$ into (46) and (47). Although the global optimality of the OFDM cannot be theoretically guaranteed for the A-ACF case, our numerical results suggested that there is no other signaling scheme produces a lower EISL than that of the OFDM.

Finally, we establish the global optimality of the SC waveform for super-Gaussian constellations in the A-ACF case.

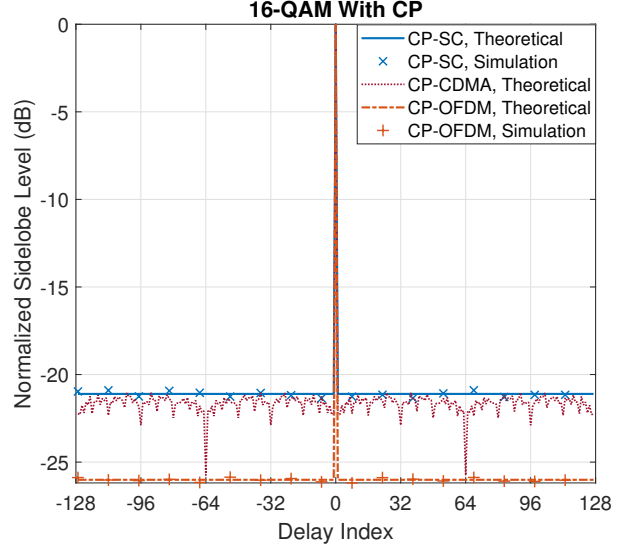


Fig. 2. The P-ACF of the 16-QAM constellation under various signaling schemes, $N = 128$.

Corollary 4. *SC waveform achieves the lowest EISL for super-Gaussian constellations in the A-ACF case.*

Proof. Again, to minimize the A-ACF sidelobe for the $\mu_4 > 2$ case, one has to minimize $\|\tilde{\mathbf{F}}_{2N} \mathbf{U}\|_4^4$ over the unitary group $\mathbb{U}(N)$. Since the minimum of the ℓ_4 norm is attained if each entry of $\tilde{\mathbf{F}}_{2N} \mathbf{U}$ has a constant modulus, $\mathbf{U} = \mathbf{I}_N$ is a global minimizer, completing the proof. ■

V. NUMERICAL RESULTS

In this section, we present numerical results to validate our theoretical analysis. In general, we compare the performance of three signaling schemes, namely, SC, OFDM, and CDMA waveforms employing Walsh codes. Note that we do not compare with OTFS since it is a 2-dimensional modulation over both delay and Doppler domains, while this paper considers 1-dimensional modulation and delay sidelobe analysis only. Due to the strict page limit, we designate the discussion of the Doppler sidelobe as our future work. We employ both QAM and PSK as examples for sub-Gaussian constellations. To construct a super-Gaussian constellation, we design a specific 64-APSK constellation consisting of 4 circles, each circle contains 16 points, whose radii are 4.54×10^{-5} , 0.0067, 0.0815 and 1.9983, respectively, leading to a kurtosis of 3.9867, and is referred to as ‘‘SG-64-APSK’’ in the legends of the figures. Moreover, all the simulation results are attained by averaging over 1000 random realizations.

We first illustrate the P-ACF of the 16-QAM and 64-QAM constellations in Fig. 2 and Fig. 3 with $N = 128$, for signaling schemes with CP addition. It can be observed that the theoretical values matched very well with the simulation results, which confirms the correctness of our derivation in Sec. III. The CP-CDMA scheme with Hadamard matrix as signaling basis performs slightly better than the CP-SC approach. Moreover, CP-OFDM achieves 5 dB sidelobe level reduction compared to the CP-SC, and also outperforms the CP-CDMA. Under

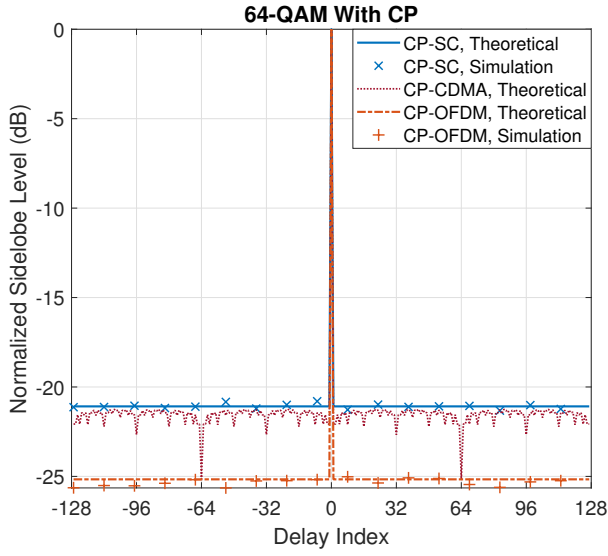


Fig. 3. The P-ACF of the 64-QAM constellation under various signaling schemes, $N = 128$.

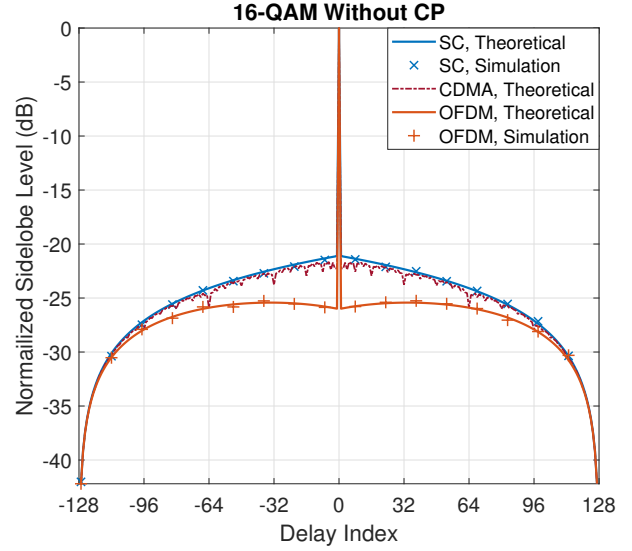


Fig. 5. The A-ACF of the 16-QAM constellation under various signaling schemes, $N = 128$.

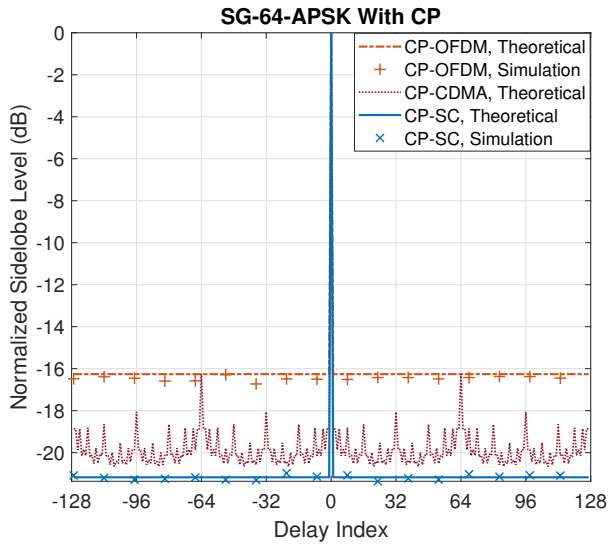


Fig. 4. The P-ACF of the 64-APSK constellation under various signaling schemes, $N = 128$.

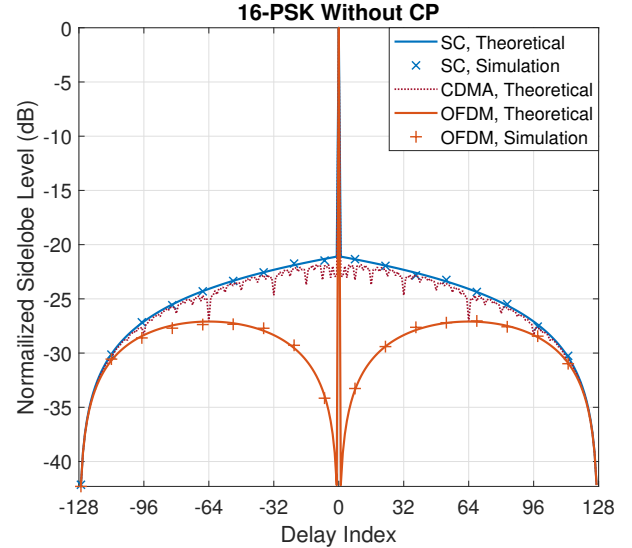


Fig. 6. The A-ACF of the 16-PSK constellation under various signaling schemes, $N = 128$.

the CP-OFDM signaling, there is a moderate increase in the sidelobe level of the 64-QAM constellation compared to that of its 16-QAM counterpart, due to the fact that 64-QAM has a higher kurtosis.

To examine the performance of the super-Gaussian constellations, we portray the P-ACF of the designed SG-64-APSK constellation in Fig. 4 under various signaling schemes. As predicted by our theoretical framework, the CP-SC now becomes the best signaling scheme among all other strategies, which attains a 5dB sidelobe reduction compared to the CP-OFDM waveform. In fact, even the CP-CDMA signal yields a lower sidelobe level than the CP-OFDM counterpart, making the latter the worst signaling basis for the super-Gaussian constellations.

We then look at the sidelobe performance of 16-QAM and

16-PSK constellations for signaling strategies without CP in Fig. 5 and Fig. 6. Again, all the theoretical results perfectly match their numerical counterparts. Moreover, the same trends may be observed in both figures, that the OFDM is superior to both SC and CDMA schemes, even if there is no global optimality guarantee for OFDM in the CP-free case. It is also interesting to highlight that for the 16-PSK constellation with OFDM signaling, the sidelobe level goes down when the delay index approaches to zero. This is because when the delay is small, the linear convolution may be approximated as a periodic convolution. In such a case, the sidelobe value of the A-ACF at those delay lags may be very close to those of its P-ACF counterpart, which is exactly zero for PSK alphabets, as discussed in Remark 2. As a comparison, the sidelobe performance of the SG-64-APSK constellation is portrayed in

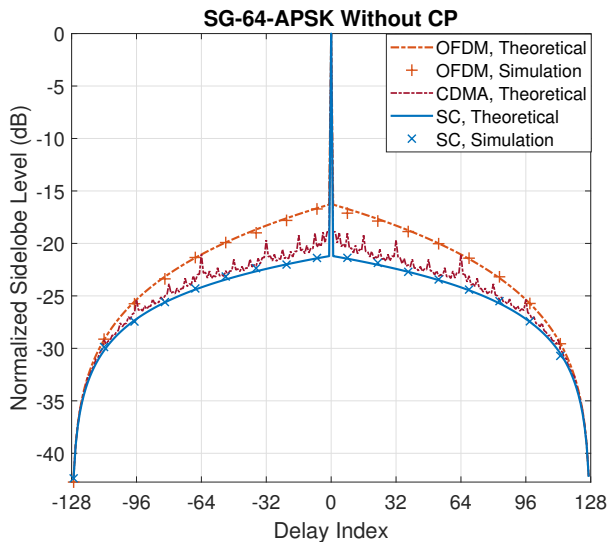


Fig. 7. The A-ACF of the 64-APSK constellation under various signaling schemes, $N = 128$.

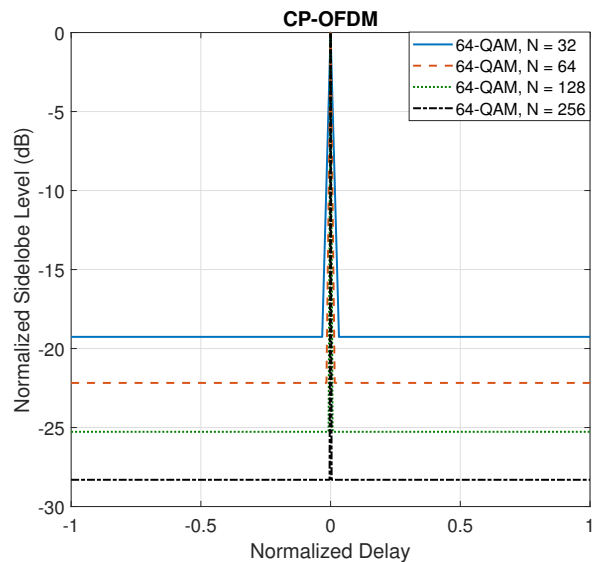


Fig. 9. The P-ACF of 64-QAM constellation under CP-OFDM signaling with varying N .

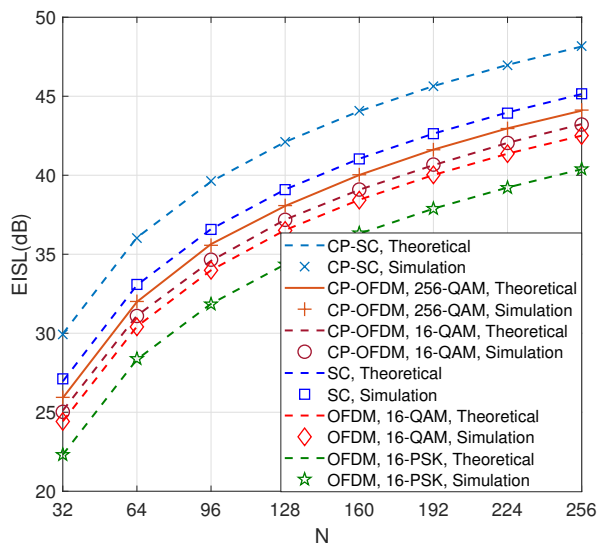


Fig. 8. The resultant EISL for different constellations under OFDM and SC signaling with varying number of symbols.

Fig. 7, under three signaling strategies without CP. It can be clearly seen that the SC scheme reaches the lowest sidelobe compared to other two waveforms, which is consistent with Corollary 4.

To show the overall performance of different signaling schemes, we illustrate the resultant EISL for different constellations under SC and OFDM waveforms in Fig. 8, where both cases with and without CP are considered. First of all, signals with CP generally lead to higher sidelobe levels compared to those without, which may also be inferred from their respective EISL expressions (29) and (42). Moreover, in both P-ACF and A-ACF cases, SC schemes result in the same EISL regardless of the choice of constellations. Higher-order QAM modulations always end up with larger sidelobe levels, owing

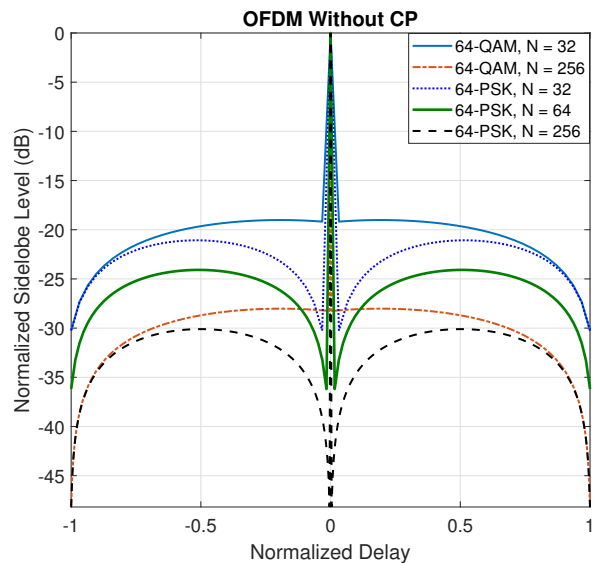


Fig. 10. The A-ACF of 64-QAM/PSK constellation under OFDM signaling with varying N .

to a larger kurtosis. As expected, PSK with OFDM signaling attains the smallest EISL of the A-ACF, despite that OFDM is only a local optimum in such a case.

Next, we investigate the scaling law of the peak-to-sidelobe level ratio (PSLR) of the OFDM signaling schemes, where both waveforms with and without CP are analyzed in Fig. 9 and Fig. 10, respectively. While the EISL increases with the number of symbols, the mainlobe levels are also on the rise. As can be seen in Fig. 9 and Fig. 10, a 3 dB performance gain in PSLR may be obtained simply by doubling N , which has already been predicted in our theoretical results. Moreover, in the CP-free case, PSK always outperforms its QAM counterpart when N keeps the same.

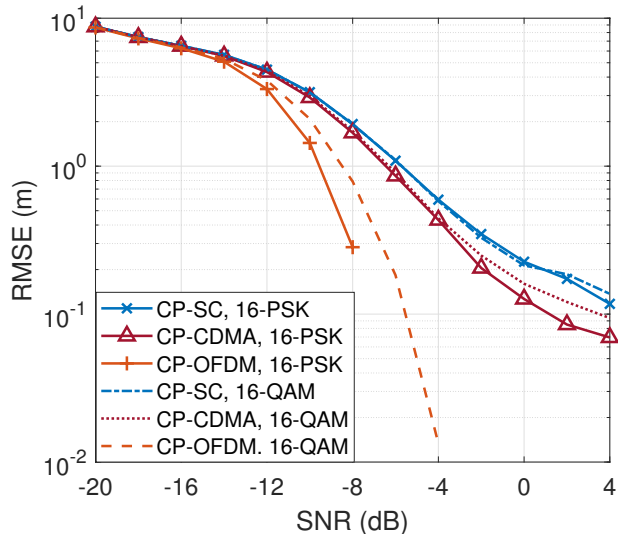


Fig. 11. Two-target ranging RMSE of different waveforms with CP for PSK and QAM modulations, with a pair of strong and weak targets located at 11.25m and 18.75m.

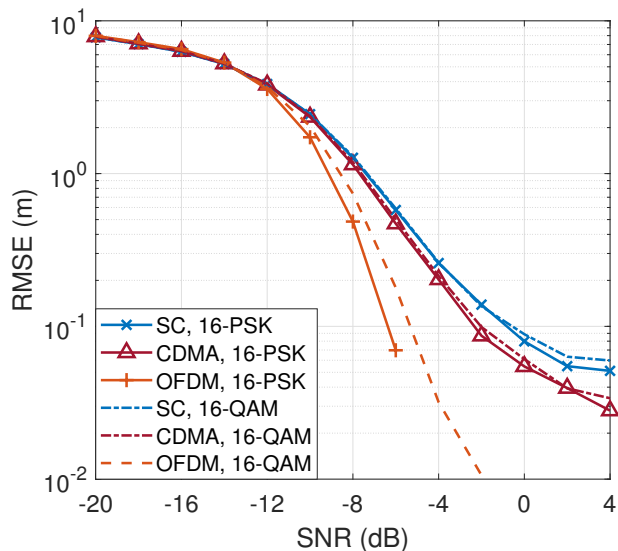


Fig. 12. Two-target ranging RMSE of different waveforms without CP for PSK and QAM modulations, with a pair of strong and weak targets located at 11.25m and 18.75m.

Finally, we examine the practical ranging performance of different waveforms under random PSK and QAM symbols in Fig. 11 and Fig. 12. In particular, we consider a ranging task where a strong target and a weak target need to be simultaneously sensed. The bandwidth of different waveforms is set as 800 MHz. By fixing the transmit power to 1, the SNR is defined as the inverse of the noise variance. The two targets are located at 11.25m and 18.75m, respectively, where the reflection power of the 11.25m target is 10 dB higher than the one at 18.75m, such that the latter may be masked by the sidelobe of the strong target with high probability. In this sense, a lower EISL intuitively indicates a better ranging performance. This intuition has been confirmed by our

simulation, where the OFDM waveform always outperforms the SC and CDMA by an order of magnitude, for both cases with and without CP. It may also be observed that PSK achieves significantly lower ranging errors compared to QAM for CP-OFDM/OFDM signaling, and a slightly better performance in the CP-CDMA/CDMA cases, despite that they exhibit almost equivalent performance under SC waveforms. These results are all consistent with their respective sidelobe levels analyzed in the above, which guarantee the usefulness of the proposed EISL as a well-defined ranging metric for random ISAC signaling.

VI. CONCLUSIONS

This study has provided a comprehensive analysis of communication-centric ISAC waveforms, specifically focusing on their sensing performance in terms of the ranging sidelobe levels. Our findings demonstrated the superiority of OFDM modulation over other waveforms in achieving the lowest ranging sidelobe, confirmed through rigorous evaluation of both aperiodic and periodic auto-correlation functions. The introduction of the expectation of the integrated sidelobe level (EISL) as a key metric has further quantified this performance, establishing OFDM as the globally optimal waveform with a cyclic prefix (CP) and a locally optimal waveform without. The theoretical proofs and numerical validations presented reinforce OFDM's pivotal role in enhancing the ranging performance of ISAC systems. Future work should explore potential enhancements in waveform design and further refine these findings by considering practical power allocation and pulse shaping designs.

APPENDIX A PROOF OF LEMMA 2

First of all, by noting that $\text{vec}(\mathbf{ss}^H) = \mathbf{s}^* \otimes \mathbf{s}$, \mathbf{S} could be written in the form of

$$\begin{aligned} \mathbf{S} &= \mathbb{E}(\tilde{\mathbf{s}}\tilde{\mathbf{s}}^H) = \mathbb{E}\{(\mathbf{s}^* \otimes \mathbf{s})(\mathbf{s}^T \otimes \mathbf{s}^H)\} \\ &= \mathbb{E}(\mathbf{s}^* \mathbf{s}^T \otimes \mathbf{ss}^H), \end{aligned} \quad (48)$$

The relationship between the entries of \mathbf{S} and those of \mathbf{s} may be given as

$$S_{k(m-1)+p, l(n-1)+q} = \mathbb{E}(s_m^* s_n s_p s_q^*), \quad k, l \in \{0, \dots, N-1\}. \quad (49)$$

By adopting the Assumptions 1 and 2, and exploiting the independence between s_n and s_m for $n \neq m$, we further obtain

$$\mathbb{E}(s_m^* s_n s_p s_q^*) = \begin{cases} \mathbb{E}(|s_n|^4) = \mu_4, & m = n = p = q, \\ \mathbb{E}(|s_n|^2)\mathbb{E}(|s_p|^2) = 1, & m = n, p = q, n \neq p, \\ \mathbb{E}(|s_m|^2)\mathbb{E}(|s_n|^2) = 1, & m = p, n = q, m \neq n, \\ \mathbb{E}(s_m^{*2})\mathbb{E}(s_n^2) = 0, & m = q, n = p, m \neq n, \\ 0, & \text{otherwise,} \end{cases} \quad (50)$$

which completes the proof.

APPENDIX B
PROOF OF PROPOSITION 1

By noting (24), the squared P-ACF may be formulated as

$$\begin{aligned} |\tilde{r}_k|^2 &= \sum_{n=1}^N |\mathbf{v}_n^H \mathbf{s}|^2 e^{-j2\pi k \frac{(n-1)}{N}} \sum_{m=1}^N |\mathbf{v}_m^H \mathbf{s}|^2 e^{j2\pi k \frac{(m-1)}{N}} \\ &= \sum_{n=1}^N \sum_{m=1}^N |\mathbf{v}_n^H \mathbf{s}|^2 |\mathbf{v}_m^H \mathbf{s}|^2 e^{-j2\pi k \frac{(n-m)}{N}}. \end{aligned} \quad (51)$$

Expanding $|\mathbf{v}_n^H \mathbf{s}|^2$ yields

$$\begin{aligned} |\mathbf{v}_n^H \mathbf{s}|^2 &= \mathbf{v}_n^H \mathbf{s} \mathbf{s}^H \mathbf{v}_n = (\mathbf{v}_n^T \otimes \mathbf{v}_n^H) \text{vec}(\mathbf{s} \mathbf{s}^H) \\ &= (\mathbf{v}_n^T \otimes \mathbf{v}_n^H) \tilde{\mathbf{s}} = \tilde{\mathbf{s}}^H (\mathbf{v}_n^* \otimes \mathbf{v}_n). \end{aligned} \quad (52)$$

Therefore,

$$\mathbb{E}(|\tilde{r}_k|^2) = \sum_{n=1}^N \sum_{m=1}^N (\mathbf{v}_n^T \otimes \mathbf{v}_n^H) \mathbf{S} (\mathbf{v}_m^* \otimes \mathbf{v}_m) e^{-j2\pi k \frac{(n-m)}{N}}, \quad (53)$$

where $\mathbf{S} = \mathbb{E}(\tilde{\mathbf{s}} \tilde{\mathbf{s}}^H)$. To simplify (53), \mathbf{S} is decomposed as

$$\mathbf{S} = \mathbf{I}_{N^2} + \mathbf{S}_1 + \mathbf{S}_2, \quad (54)$$

where

$$\mathbf{S}_1 = \text{Diag} \left([\mu_4 - 2, \mathbf{0}_N^T, \mu_4 - 2, \mathbf{0}_N^T, \dots, \mu_4 - 2]^T \right), \quad (55)$$

$$\mathbf{S}_2 = [\mathbf{c}, \mathbf{0}_{N^2 \times N}, \mathbf{c}, \dots, \mathbf{c}, \mathbf{0}_{N^2 \times N}, \mathbf{c}], \quad (56)$$

with $\mathbf{0}_{N^2 \times N}$ being the all-zero matrix of size $N^2 \times N$, and

$$\mathbf{c} = [1, \mathbf{0}_N^T, 1, \dots, 1, \mathbf{0}_N^T, 1]^T. \quad (57)$$

Due to the fact that $\mathbf{v}_n^H \mathbf{v}_m = \delta_{n,m}$, we have

$$(\mathbf{v}_n^T \otimes \mathbf{v}_n^H) \mathbf{I}_{N^2} (\mathbf{v}_m^* \otimes \mathbf{v}_m) = \mathbf{v}_n^T \mathbf{v}_m^* \mathbf{v}_n^H \mathbf{v}_m = \delta_{n,m}, \quad (58)$$

$$\begin{aligned} (\mathbf{v}_n^T \otimes \mathbf{v}_n^H) \mathbf{S}_1 (\mathbf{v}_m^* \otimes \mathbf{v}_m) &= (\mu_4 - 2) \sum_{p=1}^N |v_{p,n}|^2 |v_{p,m}|^2 \\ &= (\mu_4 - 2) \|\mathbf{v}_n \odot \mathbf{v}_m\|_2^2, \end{aligned} \quad (59)$$

$$\begin{aligned} (\mathbf{v}_n^T \otimes \mathbf{v}_n^H) \mathbf{S}_2 (\mathbf{v}_m^* \otimes \mathbf{v}_m) &= \sum_{p=1}^N |v_{p,n}|^2 \sum_{q=1}^N |v_{q,m}|^2 \\ &= \|\mathbf{v}_n\|_2^2 \|\mathbf{v}_m\|_2^2 = 1, \end{aligned} \quad (60)$$

Plugging (54), (58)-(60) into (53) immediately leads to

$$\begin{aligned} \mathbb{E}(|\tilde{r}_k|^2) &= N^2 \delta_{0,k} + N \\ &\quad + (\mu_4 - 2) \sum_{n=1}^N \sum_{m=1}^N \|\mathbf{v}_n \odot \mathbf{v}_m\|_2^2 e^{j2\pi k \frac{(n-m)}{N}}. \end{aligned} \quad (61)$$

Moreover, based on the definition of (27), we have

$$\begin{aligned} \|\mathbf{b}_k\|_2^2 &= \sum_{p=1}^N \sum_{n=1}^N \sum_{m=1}^N |v_{p,n}|^2 |v_{p,m}|^2 e^{j2\pi k \frac{(n-m)}{N}} \\ &= \sum_{n=1}^N \sum_{m=1}^N \|\mathbf{v}_n \odot \mathbf{v}_m\|_2^2 e^{j2\pi k \frac{(n-m)}{N}}. \end{aligned} \quad (62)$$

Therefore, (61) can be recast in a compact form as (26), completing the proof.

APPENDIX C
PROOF OF PROPOSITION 2

It can be noted from (27) that the p th entry of \mathbf{b}_k , namely,

$$b_{k,p} = \sum_{n=1}^N |v_{p,n}|^2 e^{-j2\pi k \frac{(n-1)}{N}} \quad (63)$$

is the DFT of the p th row of \mathbf{V} . Using the Parseval's theorem yields

$$\frac{1}{N} \sum_{k=0}^{N-1} |b_{k,p}|^2 = \sum_{n=1}^N |v_{p,n}|^4, \quad (64)$$

and hence

$$\begin{aligned} \sum_{k=0}^{N-1} \mathbb{E}(|\tilde{r}_k|^2) &= 2N^2 + (\mu_4 - 2) \sum_{k=0}^{N-1} \|\mathbf{b}_k\|_2^2 \\ &= 2N^2 + (\mu_4 - 2) \sum_{k=0}^{N-1} \sum_{p=1}^N |b_{k,p}|^2 \\ &= 2N^2 + (\mu_4 - 2) N \|\mathbf{V}\|_4^4, \end{aligned} \quad (65)$$

which implies

$$\begin{aligned} \sum_{k=1}^{N-1} \mathbb{E}(|\tilde{r}_k|^2) &= \sum_{k=0}^{N-1} \mathbb{E}(|\tilde{r}_k|^2) - \mathbb{E}(|\tilde{r}_0|^2) \\ &= N(N-1) + (\mu_4 - 2) N (\|\mathbf{F}_N \mathbf{U}\|_4^4 - 1). \end{aligned} \quad (66)$$

APPENDIX D
PROOF OF PROPOSITION 3

For notational convenience, let us define $\mathbf{A} = \mathbf{U}^H = [\mathbf{a}_1, \mathbf{a}_2, \dots, \mathbf{a}_N]$, such that the n th row of \mathbf{U} may be denoted as \mathbf{a}_n^H , and thereby $a_{m,n} = u_{n,m}^*$. Therefore we have

$$\sum_{n=1}^{N-k} a_{m,n} a_{m,n+k}^* = \sum_{n=1}^{N-k} u_{n,m}^* u_{n+k,m} = \mathbf{u}_m^H \mathbf{J}_k \mathbf{u}_m, \quad (67)$$

which is the A-ACF of \mathbf{u}_m , and thus

$$\begin{aligned} &\sum_{n=1}^{N-k} (\mathbf{a}_{n+k}^* \odot \mathbf{a}_n) \\ &= \left[\sum_{n=1}^{N-k} a_{1,n} a_{1,n+k}^*, \dots, \sum_{n=1}^{N-k} a_{N,n} a_{N,n+k}^* \right]^T \\ &= [\mathbf{u}_1^H \mathbf{J}_k \mathbf{u}_1, \dots, \mathbf{u}_N^H \mathbf{J}_k \mathbf{u}_N]^T, \end{aligned} \quad (68)$$

which implies

$$\left\| \sum_{n=1}^{N-k} (\mathbf{a}_{n+k}^* \odot \mathbf{a}_n) \right\|_2^2 = \sum_{n=1}^N |\mathbf{u}_n^H \mathbf{J}_k \mathbf{u}_n|^2. \quad (69)$$

Moreover, we have $\mathbf{x} = \mathbf{U} \mathbf{s} = [\mathbf{a}_1^H \mathbf{s}, \mathbf{a}_2^H \mathbf{s}, \dots, \mathbf{a}_N^H \mathbf{s}]^T$. The A-ACF of \mathbf{x} may be therefore expressed as

$$r_k = \mathbf{x}^H \mathbf{J}_k \mathbf{x} = \mathbf{s}^H \mathbf{A} \mathbf{J}_k \mathbf{A}^H \mathbf{s} = \sum_{n=1}^{N-k} \mathbf{a}_n^H \mathbf{s} \mathbf{s}^H \mathbf{a}_{n+k}. \quad (70)$$

With the above identities, we are now ready to present the average squared A-ACF in closed form.

From (70) we have

$$\begin{aligned} |r_k|^2 &= \sum_{n=1}^{N-k} \sum_{m=1}^{N-k} (\mathbf{a}_n^H \mathbf{S} \mathbf{S}^H \mathbf{a}_{n+k}) (\mathbf{a}_{m+k}^H \mathbf{S} \mathbf{S}^H \mathbf{a}_m) \\ &= \sum_{n=1}^{N-k} \sum_{m=1}^{N-k} (\mathbf{a}_{n+k}^T \otimes \mathbf{a}_n^H) \tilde{\mathbf{S}} \tilde{\mathbf{S}}^T (\mathbf{a}_m \otimes \mathbf{a}_{m+k}^*), \end{aligned} \quad (71)$$

where we recall $\tilde{\mathbf{s}} = \text{vec}(\mathbf{S} \mathbf{S}^H)$. In order to reuse the results in Lemma 2, one has to transform $\tilde{\mathbf{S}} \tilde{\mathbf{S}}^T$ into $\tilde{\mathbf{S}} \tilde{\mathbf{S}}^H$. This can be realized by the commutation matrix $\mathbf{K} \in \mathbb{O}(N^2)$, such that $\mathbf{K}(\mathbf{a} \otimes \mathbf{b}) = \mathbf{b} \otimes \mathbf{a}$, where $\mathbb{O}(n)$ represents the orthogonal group of degree n . Therefore,

$$\mathbf{K} \tilde{\mathbf{s}} = \mathbf{K}(\mathbf{s}^* \otimes \mathbf{s}) = \mathbf{s} \otimes \mathbf{s}^* = \tilde{\mathbf{s}}^* \Rightarrow \tilde{\mathbf{s}}^T \mathbf{K}^T = \tilde{\mathbf{s}}^H. \quad (72)$$

One may therefore recast each term in (71) as

$$\begin{aligned} &(\mathbf{a}_{n+k}^T \otimes \mathbf{a}_n^H) \tilde{\mathbf{S}} \tilde{\mathbf{S}}^T (\mathbf{a}_m \otimes \mathbf{a}_{m+k}^*) \\ &= (\mathbf{a}_{n+k}^T \otimes \mathbf{a}_n^H) \tilde{\mathbf{S}} \tilde{\mathbf{S}}^T \mathbf{K}^T \mathbf{K} (\mathbf{a}_m \otimes \mathbf{a}_{m+k}^*) \\ &= (\mathbf{a}_{n+k}^T \otimes \mathbf{a}_n^H) \tilde{\mathbf{S}} \tilde{\mathbf{S}}^H (\mathbf{a}_{m+k}^* \otimes \mathbf{a}_m). \end{aligned} \quad (73)$$

Hence, the average squared A-ACF may be formulated as

$$\mathbb{E}(|r_k|^2) = \sum_{n=1}^{N-k} \sum_{m=1}^{N-k} (\mathbf{a}_{n+k}^T \otimes \mathbf{a}_n^H) \mathbf{S} (\mathbf{a}_{m+k}^* \otimes \mathbf{a}_m), \quad (74)$$

by recalling $\mathbf{S} = \mathbb{E}(\tilde{\mathbf{S}} \tilde{\mathbf{S}}^H)$. Again, note that $\mathbf{a}_n^H \mathbf{a}_m = \delta_{n,m}$. By relying on Lemma 2 and the decomposition $\mathbf{S} = \mathbf{I}_{N^2} + \mathbf{S}_1 + \mathbf{S}_2$ in (54), we arrive at

$$(\mathbf{a}_{n+k}^T \otimes \mathbf{a}_n^H) \mathbf{I}_{N^2} (\mathbf{a}_{m+k}^* \otimes \mathbf{a}_m) = \mathbf{a}_{n+k}^T \mathbf{a}_{m+k}^* \mathbf{a}_n^H \mathbf{a}_m = \delta_{n,m}, \quad (75)$$

$$\begin{aligned} &(\mathbf{a}_{n+k}^T \otimes \mathbf{a}_n^H) \mathbf{S}_1 (\mathbf{a}_{m+k}^* \otimes \mathbf{a}_m) \\ &= (\mu_4 - 2) (\mathbf{a}_{n+k}^* \odot \mathbf{a}_n)^H (\mathbf{a}_{m+k}^* \odot \mathbf{a}_m), \end{aligned} \quad (76)$$

$$(\mathbf{a}_{n+k}^T \otimes \mathbf{a}_n^H) \mathbf{S}_2 (\mathbf{a}_{m+k}^* \otimes \mathbf{a}_m) = \mathbf{a}_{n+k}^T \mathbf{a}_n^* \mathbf{a}_{m+k}^H \mathbf{a}_m = \delta_{0,k}. \quad (77)$$

Plugging (54), (69), (75)-(77) to (74), we obtain (41).

APPENDIX E PROOF OF PROPOSITION 4

It can be straightforwardly deduced from (41) that

$$\begin{aligned} \sum_{k=1}^{N-1} \mathbb{E}(|r_k|^2) &= \sum_{k=1}^{N-1} (N-k) + (\mu_4 - 2) \sum_{k=1}^{N-1} \sum_{n=1}^N |\mathbf{u}_n^H \mathbf{J}_k \mathbf{u}_n|^2 \\ &= \frac{N(N-1)}{2} + (\mu_4 - 2) \sum_{n=1}^N \sum_{k=1}^{N-1} |\mathbf{u}_n^H \mathbf{J}_k \mathbf{u}_n|^2, \end{aligned} \quad (78)$$

where $\sum_{k=1}^{N-1} |\mathbf{u}_n^H \mathbf{J}_k \mathbf{u}_n|^2$ is the ISL of the A-ACF of \mathbf{u}_n . According to [38], the ISL of a deterministic sequence $\mathbf{u}_n = [u_{1,n}, \dots, u_{N,n}]^T$ may be equivalently written as

$$\begin{aligned} \sum_{k=1}^{N-1} |\mathbf{u}_n^H \mathbf{J}_k \mathbf{u}_n|^2 &= \frac{1}{4N} \sum_{p=1}^{2N} \left(\left| \sum_{q=1}^N u_{q,n} e^{-\frac{j2\pi pq}{2N}} \right|^2 - 1 \right)^2 \\ &= \frac{1}{4N} \sum_{p=1}^{2N} \left(\left| \sum_{q=1}^N u_{q,n} e^{-\frac{j2\pi pq}{2N}} \right|^4 - 2 \left| \sum_{q=1}^N u_{q,n} e^{-\frac{j2\pi pq}{2N}} \right|^2 + 1 \right), \end{aligned} \quad (79)$$

where

$$\begin{aligned} \sum_{p=1}^{2N} \left| \sum_{q=1}^N u_{q,n} e^{-\frac{j2\pi pq}{2N}} \right|^4 &= 4N^2 \left\| \tilde{\mathbf{F}}_{2N} \mathbf{u}_n \right\|_4^4, \\ \sum_{p=1}^{2N} \left| \sum_{q=1}^N u_{q,n} e^{-\frac{j2\pi pq}{2N}} \right|^2 &= 2N \left\| \tilde{\mathbf{F}}_{2N} \mathbf{u}_n \right\|_2^2 = 2N. \end{aligned} \quad (80)$$

Therefore

$$\begin{aligned} \sum_{n=1}^N \sum_{k=1}^{N-1} |\mathbf{u}_n^H \mathbf{J}_k \mathbf{u}_n|^2 &= \sum_{n=1}^N \left(N \left\| \tilde{\mathbf{F}}_{2N} \mathbf{u}_n \right\|_4^4 - \frac{1}{2} \right) \\ &= N \left(\left\| \tilde{\mathbf{F}}_{2N} \mathbf{U} \right\|_4^4 - \frac{1}{2} \right). \end{aligned} \quad (81)$$

Substituting (81) into (78) yields (42), completing the proof.

REFERENCES

- [1] M. Chafii, L. Bariah, S. Muhaidat, and M. Debbah, "Twelve scientific challenges for 6G: Rethinking the foundations of communications theory," *IEEE Commun. Surveys Tuts.*, vol. 25, no. 2, pp. 868–904, Secondquarter 2023.
- [2] W. Saad, M. Bennis, and M. Chen, "A vision of 6G wireless systems: Applications, trends, technologies, and open research problems," *IEEE Network*, vol. 34, no. 3, pp. 134–142, 2019.
- [3] F. Liu, Y. Cui, C. Masouros, J. Xu, T. X. Han, Y. C. Eldar, and S. Buzzi, "Integrated sensing and communications: Toward dual-functional wireless networks for 6G and beyond," *IEEE J. Sel. Areas Commun.*, vol. 40, no. 6, pp. 1728–1767, 2022.
- [4] ITU-R WP5D, "Draft New Recommendation ITU-R M. [IMT. Framework for 2030 and Beyond]," 2023.
- [5] Y. Cui, F. Liu, X. Jing, and J. Mu, "Integrating sensing and communications for ubiquitous iot: Applications, trends, and challenges," *IEEE Network*, vol. 35, no. 5, pp. 158–167, 2021.
- [6] Y. Liu, J. Zhang, Y. Zhang, Z. Yuan, and G. Liu, "A shared cluster-based stochastic channel model for integrated sensing and communication systems," *IEEE Trans. Veh. Technol.*, vol. 73, no. 5, pp. 6032–6044, 2024.
- [7] J. Zhang, J. Wang, Y. Zhang, Y. Liu, Z. Chai, G. Liu, and T. Jiang, "Integrated sensing and communication channel: Measurements, characteristics, and modeling," *IEEE Commun. Mag.*, vol. 62, no. 6, pp. 98–104, 2024.
- [8] F. Liu, Y.-F. Liu, A. Li, C. Masouros, and Y. C. Eldar, "Cramér-Rao bound optimization for joint radar-communication beamforming," *IEEE Trans. Signal Process.*, vol. 70, pp. 240–253, 2022.
- [9] Z. Wei, H. Qu, Y. Wang, X. Yuan, H. Wu, Y. Du, K. Han, N. Zhang, and Z. Feng, "Integrated sensing and communication signals toward 5G-A and 6G: A survey," *IEEE Internet Things J.*, vol. 10, no. 13, pp. 11 068–11 092, 2023.
- [10] Z. Wei, Y. Wang, L. Ma, S. Yang, Z. Feng, C. Pan, Q. Zhang, Y. Wang, H. Wu, and P. Zhang, "5G PRS-based sensing: A sensing reference signal approach for joint sensing and communication system," *IEEE Trans. Veh. Technol.*, vol. 72, no. 3, pp. 3250–3263, 2023.
- [11] F. Liu, L. Zheng, Y. Cui, C. Masouros, A. P. Petropulu, H. Griffiths, and Y. C. Eldar, "Seventy years of radar and communications: The road from separation to integration," *IEEE Signal Process. Mag.*, vol. 40, no. 5, pp. 106–121, 2023.
- [12] Y. Xiong, F. Liu, K. Wan, W. Yuan, Y. Cui, and G. Caire, "From torch to projector: Fundamental tradeoff of integrated sensing and communications," *IEEE BITS Inf. Theory Mag.*, pp. 1–13, 2024.
- [13] Y. Xiong, F. Liu, Y. Cui, W. Yuan, T. X. Han, and G. Caire, "On the fundamental tradeoff of integrated sensing and communications under Gaussian channels," *IEEE Trans. Inf. Theory*, vol. 69, no. 9, pp. 5723–5751, 2023.
- [14] P. Kumari, J. Choi, N. González-Prelcic, and R. W. Heath, "IEEE 802.11ad-based radar: An approach to joint vehicular communication-radar system," *IEEE Trans. Veh. Technol.*, vol. 67, no. 4, pp. 3012–3027, Apr. 2018.
- [15] P. Banelli, S. Buzzi, G. Colavolpe, A. Modenini, F. Rusek, and A. Ugolini, "Modulation formats and waveforms for 5G networks: Who will be the heir of OFDM?" *IEEE Signal Process. Mag.*, vol. 31, no. 6, pp. 80–93, 2014.

- [16] B. Popovic, "Spreading sequences for multicarrier CDMA systems," *IEEE Trans. Commun.*, vol. 47, no. 6, pp. 918–926, 1999.
- [17] R. Hadani, S. Rakib, M. Tsatsanis, A. Monk, A. J. Goldsmith, A. F. Molisch, and R. Calderbank, "Orthogonal time frequency space modulation," in *Proc. IEEE Wireless Commun. Network Conf. (WCNC)*, 2017, pp. 1–6.
- [18] Z. Wei, W. Yuan, S. Li, J. Yuan, G. Bharatula, R. Hadani, and L. Hanzo, "Orthogonal time-frequency space modulation: A promising next-generation waveform," *IEEE Wireless Commun.*, vol. 28, no. 4, pp. 136–144, 2021.
- [19] A. Bemani, N. Ksairi, and M. Kountouris, "Affine frequency division multiplexing for next generation wireless communications," *IEEE Trans. Wireless Commun.*, vol. 22, no. 11, pp. 8214–8229, 2023.
- [20] —, "Integrated sensing and communications with affine frequency division multiplexing," *IEEE Wireless Commun. Lett.*, vol. 13, no. 5, pp. 1255–1259, 2024.
- [21] C. Sturm and W. Wiesbeck, "Waveform design and signal processing aspects for fusion of wireless communications and radar sensing," *Proc. IEEE*, vol. 99, no. 7, pp. 1236–1259, Jul. 2011.
- [22] X. Chen, Z. Feng, Z. Wei, P. Zhang, and X. Yuan, "Code-division OFDM joint communication and sensing system for 6G machine-type communication," *IEEE Internet Things J.*, vol. 8, no. 15, pp. 12 093–12 105, 2021.
- [23] Y. Zeng, Y. Ma, and S. Sun, "Joint radar-communication with cyclic prefixed single carrier waveforms," *IEEE Trans. Veh. Technol.*, vol. 69, no. 4, pp. 4069–4079, 2020.
- [24] L. Chen, J. Pan, J. Zhang, J. Cheng, L. Xu, and N. Ye, "FDSS-based DFT-s-OFDM for 6G wireless sensing," *Sensors*, vol. 23, no. 3, p. 1495, 2023.
- [25] L. Gaudio, M. Kobayashi, G. Caire, and G. Colavolpe, "On the effectiveness of OTFS for joint radar parameter estimation and communication," *IEEE Trans. Wireless Commun.*, vol. 19, no. 9, pp. 5951–5965, 2020.
- [26] W. Yuan, L. Zhou, S. K. Dehkordi, S. Li, P. Fan, G. Caire, and H. V. Poor. (2023) "From OTFS to DD-ISAC: Integrating sensing and communications in the delay doppler domain". [Online]. Available: <https://arxiv.org/abs/2311.15215>
- [27] D. Tagliaferri, M. Mizmizi, S. Mura, F. Linsalata, D. Scazzoli, D. Badini, M. Magarini, and U. Spagnolini, "Integrated sensing and communication system via dual-domain waveform superposition," *IEEE Tran. Wireless Commun.*, vol. 23, no. 5, pp. 4284–4299, 2024.
- [28] N. Ishikawa, S. Sugiura, and L. Hanzo, "50 years of permutation, spatial and index modulation: From classic rf to visible light communications and data storage," *IEEE Commun. Surv. Tut.*, vol. 20, no. 3, pp. 1905–1938, 2018.
- [29] E. Basar, M. Wen, R. Mesleh, M. Di Renzo, Y. Xiao, and H. Haas, "Index modulation techniques for next-generation wireless networks," *IEEE Access*, vol. 5, pp. 16 693–16 746, 2017.
- [30] I. Abou-Faycal, M. Trott, and S. Shamai, "The capacity of discrete-time memoryless rayleigh-fading channels," *IEEE Trans. Inf. Theory*, vol. 47, no. 4, pp. 1290–1301, 2001.
- [31] M. Gursoy, H. Poor, and S. Verdu, "The noncoherent Rician fading channel-part I: Structure of the capacity-achieving input," *IEEE Trans. Wireless Commun.*, vol. 4, no. 5, pp. 2193–2206, 2005.
- [32] —, "Noncoherent Rician fading channel-part II: Spectral efficiency in the low-power regime," *IEEE Trans. Wireless Commun.*, vol. 4, no. 5, pp. 2207–2221, 2005.
- [33] R. Derryberry, S. Gray, D. Ionescu, G. Mandyam, and B. Raghathan, "Transmit diversity in 3G CDMA systems," *IEEE Commun. Mag.*, vol. 40, no. 4, pp. 68–75, 2002.
- [34] M. F. Keskin, C. Marcus, O. Eriksson, A. Alvarado, J. Widmer, and H. Wymeersch, "Integrated sensing and communications with MIMO-OTFS: ISI/ICI exploitation and delay-Doppler multiplexing," *IEEE Trans. Wireless Commun.*, pp. 1–1, 2024.
- [35] D. Falconer, S. Ariyavisitakul, A. Benyamin-Seeyar, and B. Eidson, "Frequency domain equalization for single-carrier broadband wireless systems," *IEEE Commun. Mag.*, vol. 40, no. 4, pp. 58–66, 2002.
- [36] C. Xiao, Y. R. Zheng, and Z. Ding, "Globally optimal linear precoders for finite alphabet signals over complex vector Gaussian channels," *IEEE Trans. Signal Process.*, vol. 59, no. 7, pp. 3301–3314, 2011.
- [37] P. Stoica, H. He, and J. Li, "On designing sequences with impulse-like periodic correlation," *IEEE Signal Process. Lett.*, vol. 16, no. 8, pp. 703–706, 2009.
- [38] —, "New algorithms for designing unimodular sequences with good correlation properties," *IEEE Trans. Signal Process.*, vol. 57, no. 4, pp. 1415–1425, 2009.
- [39] J. Song, P. Babu, and D. P. Palomar, "Optimization methods for designing sequences with low autocorrelation sidelobes," *IEEE Trans. Signal Process.*, vol. 63, no. 15, pp. 3998–4009, 2015.
- [40] S. Taner and C. Studer, "Optimality of the discrete Fourier transform for beamspace massive MU-MIMO communication," in *Proc. IEEE Int. Symp. Inf. Theory (ISIT)*, 2021, pp. 2960–2965.
- [41] Y. Zhai, Z. Yang, Z. Liao, J. Wright, and Y. Ma, "Complete dictionary learning via l_4 -norm maximization over the orthogonal group," *J. Mach. Learn. Res.*, vol. 21, no. 165, pp. 1–68, 2020.
- [42] C. Studer, P. Luethi, and W. Fichtner, "VLSI architecture for data-reduced steering matrix feedback in MIMO systems," in *Proc. IEEE Int. Symp. Circuits Syst. (ISCAS)*, 2008, pp. 300–303.